Effect of hydrogen dilution on carrier transport in hydrogenated boron-doped nanocrystalline silicon-silicon carbide alloys

Seung Yeop Myong[a] and Koeng Su Lim
Department of Electrical Engineering and Computer Science, Korea Advanced Institute of Science and Technology, 373-1 Guseong-dong, Yuseong-gu, Daejeon 305-701 Republic of Korea

Makoto Konagai
Department of Physical Electronics, Tokyo Institute of Technology, 2-12-1 O-okayama, Meguro-ku, Tokyo 152-8552 Japan

(Received 3 October 2005; accepted 18 January 2006; published online 10 March 2006)

The effect of the hydrogen dilution ratio on characteristics of hydrogenated boron-doped nanocrystalline silicon-silicon carbide alloy (*p*-nc-Si–SiC:H) films is investigated. Hydrogen coverage near the growing surface causes nanocrystallization by retarding the reactions of the precursors. It was found that *p*-nc-Si–SiC:H alloys have two different kinds of carrier transport mechanisms: one is the thermally activated hopping conduction between neighboring crystallites near room temperature and the other is the band tail hopping conduction below 150 K. However, the film at the onset of the nanocrystalline growth exhibits a different behavior due to a large band tail disorder. © *2006 American Institute of Physics*. [DOI: 10.1063/1.2177641]

To improve the *p*/*i* interface of thin-film silicon (Si) solar cells, we proposed an inhomogeneous hydrogenated boron (B)-doped nanocrystalline silicon-silicon carbide (*p*-nc-Si–SiC:H) alloy films. This material contains nc-Si grains embedded in a hydrogenated amorphous silicon carbide(*a*-SiC:H) matrix via a mercury (Hg)-sensitized photo-assisted chemical-vapor deposition (photo-CVD) technique, combining the photodecomposition of ethylene (C_2H_4) and hydrogen (H_2) dilution.[1] As the photo-CVD technique is ion-damage-free due to its mild process [the intensity of ultraviolet (UV) light irradiation: ~10 mW/cm^2],[1] the fabricated mixed-phase alloys are highly conductive and transparent.[2,3] Therefore, the possibility of *p*-nc-Si–SiC:H alloy films as window layers of thin-film Si solar cells was confirmed.[4] Based on the deposition of the *p*-nc-Si–SiC:H alloys, H_2-diluted *p*-*a*-SiC:H buffer layers of *pin*-type amorphous silicon (*a*-Si:H) and protocrystalline silicon (pc-Si:H) multilayer solar cells were prepared.[5–8] Accordingly, a dramatic improvement of all solar cell parameters was achieved by effectively reducing the recombination loss at the *p*/*i* interface. However, a more detailed study is required on the nature of the mixed-phase *p*-nc-Si–SiC:H alloy films that would have the best deposition conditions for photovoltaic application. A previous report by the authors introduced the temperature dependence of the direct current (dc) dark conductivity (σ_D) of *p*-nc-Si–SiC:H alloy films prepared with a different B doping ratio [diborane/silane (B_2H_6/SiH_4)].[9] In this study, we investigate the effect of the H_2 dilution on the structural and carrier transport characteristics of the *p*-nc-Si–SiC:H alloy films.

The films were deposited by the Hg-sensitized photo-CVD technique using a mixture of SiH_4, H_2, B_2H_6, and C_2H_4 reactant gases. A low-pressure Hg lamp with resonance lines of 184.9 and 253.7 nm was used as an UV light source to dissociate the mixture gases. In all depositions, the B_2H_6/SiH_4 value, ethylene gas flow ratio (C_2H_4/SiH_4), chamber pressure, substrate temperature, and Hg bath temperature were kept at 1000 ppm, 0.07, 0.46 Torr, at 250 °C, and 20 °C, respectively. The values of B_2H_6/SiH_4 and C_2H_4/SiH_4 were the same as the values of the optimum deposition condition for the H_2-diluted *p*-*a*-SiC:H buffer layers of the solar cells.[5–8] Approximately 150 nm thick films were deposited on Corning 7059 glass substrates with a varying hydrogen dilution ratio (H_2/SiH_4). The deposition rate of the films gradually decreased from 1.9 to 1.0 nm/min with the increase in H_2/SiH_4 from 15 to 30.

To inspect the structural change, we measured the selected-area transmission electron diffraction (SAED) images of the films. We also performed Raman spectroscopy (JASCO Corp., NRS-1000 system) using an Ar laser with a wavelength of 532 nm. The Raman collection depth at this wavelength is ~50 nm for *a*-Si:H and 120–170 nm for the hydrogenated microcrystalline silicon (μc-Si:H).[10] The details for the σ_D measurements were introduced in a previous report.[9]

Figure 1 shows the SAED images of the *p*-nc-Si–SiC:H alloy films prepared with different H_2/SiH_4. In

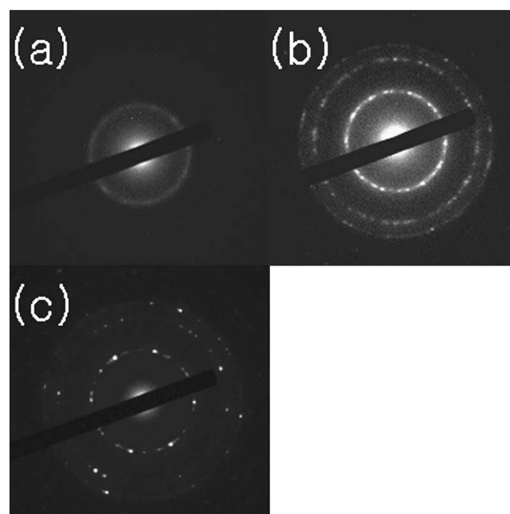

FIG. 1. SAED images of the *p*-nc-Si–SiC:H alloy films prepared at different H_2/SiH_4 conditions: (a) H_2/SiH_4=15, (b) H_2/SiH_4=20, and (c) H_2/SiH_4=25.

[a]Electronic mail: myongsy@kaist.ac.kr

 © 2006 American Institute of Physics
Downloaded 18 Apr 2011 to 143.248.224.33. Redistribution subject to AIP license or copyright; see http://apl.aip.org/about/rights_and_permissions

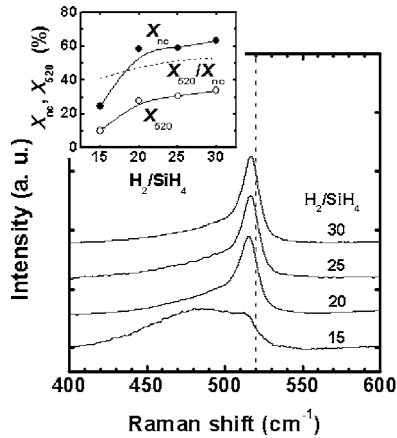

FIG. 2. Raman spectra of the *p*-nc-Si–SiC:H alloy films. The inset graph shows the crystal volume fractions of the films.

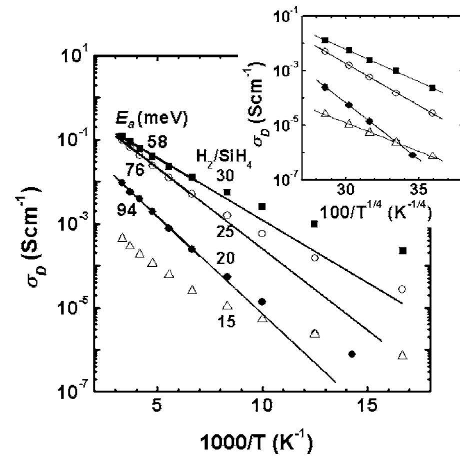

FIG. 3. Arrhenius plot for σ_D of the *p*-nc-Si–SiC:H films.

the case of $H_2/SiH_4=15$, three dim rings were detected from the center corresponding to planes (111), (220), and (311) of crystalline Si (*c*-Si). In the case of $H_2/SiH_4=20$, bright spots on the three broad rings were detected. With a further increase in H_2/SiH_4, the SAED image shows bright spots on the three sharp rings, which indicate highly oriented *c*-Si growth in the film.

Figure 2 displays the results of the Raman spectroscopy of the *p*-nc-Si–SiC:H alloy films. The deconvolution of each spectrum in Fig. 2 shows three independent peaks: (i) a transverse optical (TO) mode of the nc-Si component near 520 cm^{-1}, (ii) an intermediate fraction near 510 cm^{-1} due to small crystallites and a defective part of the crystalline phase,[10] and (iii) a TO-like *a*-Si:H phase near 480 cm^{-1}, which is related to the Si–Si bonds in *a*-SiC:H. No Raman peak associated with a crystalline silicon carbide (*c*-SiC) phase was observed in the range of 750–950 cm^{-1}. However, a Fourier transform infrared (FTIR) spectrum exhibits very small local vibrational modes of SiC at ~657 and ~789 cm^{-1}, which confirm the formation of SiC.[1] These films possess approximately 1–2 at. % C, which was roughly determined from the Auger results.[1] From the data, it is possible to conclude that the film consists of nc-Si grains embedded in an *a*-SiC:H matrix. The increase in H_2/SiH_4 induces the nanocrystalline growth by suppressing the broad *a*-SiC:H peak. The average grain size (L) of the films is estimated using a deviation ($\Delta\omega$) of the nc-Si TO peak from the frequency of the *c*-Si To peak (520 cm^{-1});[11] $L=2\pi(2/\Delta\omega)^{1/2}$. With the increase in H_2/SiH_4, the L value increases from 3.8 to 5.7 nm.

The degree of crystallinity is indicated by the crystal volume fraction (X_{nc}). In addition, the X_{520} value is evaluated in order to monitor the dominant crystal component. Since L of all the films is only 3–6 nm, X_{nc}, i.e., $X_{nc}=(I_{510}+I_{520})/(I_{480}+I_{510}+I_{520})$, where I_i denotes an integrated intensity at i cm^{-1}, and X_{520}, i.e., $X_{520}=I_{520}/(I_{480}+I_{510}+I_{520})$, can be found assuming the Raman cross-section ratio to be 1. As shown in the inset graph of Fig. 2, both the X_{nc} and X_{520} values are gradually enhanced with the increase in H_2/SiH_4. In the case of $H_2/SiH_4=15$, the film shows the onset of the nanocrystalline growth. With an increase in H_2/SiH_4 to 20, X_{nc} is abruptly elevated. In contrast, with a further increase in H_2/SiH_4, X_{nc} shows a small increase, and the nc-Si TO peak becomes dominative ($X_{520}/X_{nc}\geqslant 0.5$) due to the formation of large grains ($L\geqslant 5$ nm) and the reduction of the defective crystalline phase.[10]

From the results, it is reasonable to assume that the H_2 dilution of SiH_4 during the film deposition causes hydrogen coverage of the growing film surface.[12] This process enhances the surface diffusion coefficient of the precursors decomposed by the UV illumination, initiating precursors adsorbed at the growing surface to find their energetically suitable sites.[13] This results in a retardation of the deposition rate, which decreases the structural disorder in the film by relaxing the *a*-SiC:H matrix, and causes the generation of crystallites.

Figure 3 depicts the temperature (T) dependence of σ_D for films prepared with different H_2/SiH_4. The σ_D measured at room temperature reveals a gradual increase with the increments of H_2/SiH_4, due to the increase in the crystallinity.[1] The experimental data indicate that the conduction mechanism in the films under consideration is closely related to X_{nc} influenced by H_2/SiH_4. With the exception of the film prepared at $H_2/SiH_4=15$, the different slopes of the experimental curves in the low- and high-temperature regions point to different mechanisms of carrier transport. The straight lines approximating the experimental points for $T>150$ K reveal a thermally activated process,[14]

$$\sigma_D(T)=\sigma_o \exp(-E_a/kT), \quad (1)$$

where σ_o is the conductivity prefactor, E_a is the activation energy, and k is Boltzmann's constant. E_a values extracted using Eq. (3) are listed in this figure. It is seen that E_a decreases with an increase in H_2/SiH_4 due to the formation of highly crystalline and conductive films. In this temperature regime ($T>150$ K), we previously reported that σ_D of the highly crystalline films generally obeyed the Meyer-Neldel rule (MNR), and that carrier transport was dominated not by the extended-states transport (which was the main transport mechanism in conventional *a*-Si:H), but by thermally activated hopping between neighboring crystallites.[9] However, the film at the onset of the nanocrystalline growth ($H_2/SiH_4=15$) reveals the different transport behavior of a continuous bending in this temperature regime. We attribute the continuous bending with the temperature to a large band tail disorder.[15]

Below 150 K, all of the *p*-nc-Si–SiC:H alloy films display a linear relationship between log σ_D and $T^{1/4}$, as shown in the inset graph of Fig. 3. This behavior is consistent with

Downloaded 18 Apr 2011 to 143.248.224.33. Redistribution subject to AIP license or copyright; see http://apl.aip.org/about/rights_and_permissions

TABLE I. Values of DOS calculated from the percolation model for the p-nc-Si–SiC:H alloy films.

H_2/SiH_4	σ_{oo} (Ω^{-1} cm^{-1})	T_0^* (K)	$G(E)$ (eV^{-1}cm^{-3}) (C_0=16)	$G(E)$ (eV^{-1}cm^{-3}) (C_0=310)
15	2.49×10^{1}	2.49×10^{6}	3.37×10^{19}	6.53×10^{20}
20	1.84×10^{8}	8.35×10^{7}	2.22×10^{18}	4.31×10^{19}
25	3.42×10^{6}	2.57×10^{7}	7.23×10^{18}	1.40×10^{20}
30	8.17×10^{4}	8.98×10^{6}	2.07×10^{19}	5.01×10^{20}

a variable range hopping (VRH) model known to be limited to a low-temperature region.[16] In this temperature region, σ_D follows Mott's law,[17] where the carrier transport is dominated by the VRH hopping process in a constant density of states (DOS) near the Fermi level (E_F),

$$\sigma_D = \sigma_{oo} \exp[-(T_0/T)^{1/4}]. \quad (2)$$

In the classical Mott's model, the σ_{oo} and T_0 coefficients are given by

$$\sigma_{oo} = e^2 N(E_F)\gamma_{\mathrm{ph}}/\alpha^2, \quad (3)$$

$$T_0 = 16\alpha^3/kN(E_F), \quad (4)$$

where e is the electron charge, γ_{ph} is the characteristic phonon frequency, α is the inverse decay length of the wave function of localized states near E_F, and $N(E_F)$ is the concentration of these localized states at E_F. However, this model with a constant DOS leads to improbable $N(E_F)$ for disordered thin films with exponential tail state distributions in the gap.[18] Hence, this model must be corrected to achieve rational $N(E_F)$.

Godet[19] predicted that using the localization radius as a parameter $[10^{-5} < N(E_F)\alpha^{-3} < 1]$ a single-phonon band tail hopping within an exponential DOS gives a linear relationship between $\ln \sigma_{oo}$ and $T_0^{1/4}$. Concari *et al.*[20] provided the validity of Godet's model for i-μc-Si:H and p-μc-Si:H by correlating the classical percolation theory,[21]

$$T_0^* = C_0\alpha^3/kg(E_F), \quad (5)$$

where C_0 is a constant with a value in the range of 16 (Ref. 21) to 310 (Ref. 19) and $g(E_F)$ is the unitary energy DOS with an exponential distribution near E_F in Godet's model. Here, α^{-1} typically varies between 0.3 and 3 nm.

From Eq. (5), it is possible to estimate the $g(E_F)$ value of the p-nc-Si–SiC:H alloy films by assuming α^{-1} to be 1 nm.[20,22] The calculated parameters are presented in Table I. The film at the onset of the nanocrystalline growth (H_2/SiH_4=15) has the highest DOS, which supports the assumption of many defects and structural disorder in the film. With the increase in H_2/SiH_4 from 15 to 20, the value of $g(E_F)$) for the p-nc-Si–SiC:H alloy films is steeply reduced by an order of magnitude. The reduction is ascribed to the decrease in the volume fraction of the a-SiC:H matrix. However, with a further increase in H_2/SiH_4, the value of $g(E_F)$ for the highly nanocrystalline films gradually increases, due to the enhanced distribution of dangling bond states in the grain boundary regions and the enhanced ionized impurities near E_F.

On the other hand, Ram *et al.*[15] suggested a $T^{-1/2}$ dependence on the log σ_D of fully crystallize i-μc-Si:H films in the low-temperature region of 80–300 K. They attributed this behavior to the tunneling of carriers through barriers similar to what is observed in granular metals. Thus, the $T^{-1/2}$ dependence on the log σ_D of the p-nc-Si–SiC:H alloy films was checked at this point in this study. Although the defective film deposited at H_2/SiH_4=15 shows a good linear fit near room temperature, this fitting method makes a considerable deviation of all the samples in the very low-temperature region below 150 K. Therefore, it is concluded that the aforementioned fitting method is better than the method suggested by Ram *et al.* for the mixed-phased p-nc-Si–SiC:H alloy films. The recent finding by Dussan *et al.*,[22] which presents a very good $T^{-1/4}$ dependence on the log σ_D of p-μc-Si:H films in the low-temperature range of 120–300 K, supports our conclusion.

Finally a good linear relationship between $\ln \sigma_{oo}$ and $T_0^{*1/4}$ of the p-nc-Si–SiC:H alloy films, including data in Ref. 9 is found. Interestingly, the relationship is almost identical to the linear relationship of i-μc-Si:H and p-μc-Si:H.[20] This result supports the validity of Godet's model.

In summary, it is found that H_2/SiH_4 significantly impacts the level of E_F and the DOS formation in the films. From the results of dc σ_D measured over the temperature range of 60–300 K, two different kinds of the carrier transport mechanisms of the highly crystalline p-nc-Si–SiC:H alloy films were observed; the thermally activated mechanism mainly due to intercrystallite hopping near the room-temperature region, and the band tail hopping mechanism below 150 K. However, the film prepared at the onset of the nanocrystalline growth (with the low H_2/SiH_4 value of 15) reveals the continuous bending near room temperature primary due to the large band tail disorder.

[1] S. Y. Myong, H. K. Lee, E. Yoon, and K. S. Lim, J. Non-Cryst. Solids **298**, 131 (2002).
[2] S. Y. Myong, O. Shevaleevskiy, S. Miyajima, M. Konagai, and K. S. Lim, J. Non-Cryst. Solids **351**, 89 (2005).
[3] H. K. Lee, S. Y. Myong, K. S. Lim, and E. Yoon, J. Non-Cryst. Solids **316**, 297 (2003).
[4] S. Y. Myong, T. H. Kim, K. H. Kim, B. T. Ahn, S. Miyajima, M. Konagai, and K. S. Lim, Sol. Energy Mater. Sol. Cells **81**, 485 (2004).
[5] S. Y. Myong, S. S. Kim, and K. S. Lim, J. Appl. Phys. **95**, 1525 (2004).
[6] S. Y. Myong and K. S. Lim, Appl. Phys. Lett. **86**, 033506 (2005).
[7] S. Y. Myong, S. W. Kwon, M. Konagai, and K. S. Lim, Sol. Energy Mater. Sol. Cells **85**, 133 (2005).
[8] S. Y. Myong, J. M. Pearce, M. Konagai, and K. S. Lim, Appl. Phys. Lett. **87**, 193509 (2005); S. Y. Myong, S. W. Kwon, M. Kondo, M. Konagai, and K. S. Lim, Semicond. Sci. Technol. **21**, L11 (2006).
[9] S. Y. Myong, O. Shevaleevskiy, S. Miyajima, M. Konagai, and K. S. Lim, J. Appl. Phys. **98**, 054311 (2005).
[10] C. Droz, E. Vallat-Sauvain, J. Bailat, L. Feitknecht, J. Meier, and A. Shah, Sol. Energy Mater. Sol. Cells **81**, 61 (2004).
[11] Y. He, C. Yin, G. Cheng, L. Wang, X. Liu, and G. Y. Hu, J. Appl. Phys. **60**, 673 (1993).
[12] S. Ghosh, A. De, S. Ray, and A. K. Barua, J. Appl. Phys. **71**, 5205 (1992).
[13] A. Matsuda, J. Non-Cryst. Solids **59/60**, 767 (1983).
[14] W. Meyer and H. Neldel, Z. Tech. Phys. (Leipzig) **12**, 588 (1937).
[15] S. K. Ram, S. Kumar, R. Vanderhaghen, and P. R. i Cabarrocas, J. Non-Cryst. Solids **299–302**, 411 (2002).
[16] N. F. Mott, J. Non-Cryst. Solids **1**, 1 (1968).
[17] N. F. Mott, *Metal-Insulator Transitions* (Taylor & Francis, London, 1990).
[18] A. Helmbold, P. Hammer, J. U. Thiele, K. Rohwer, and D. Meissner, Philos. Mag. B **72**, 335 (1995).
[19] C. Godet, J. Non-Cryst. Solids **299–302**, 333 (2002).
[20] S. B. Concari, R. H. Buitrago, M. T. Gutiérrez, and J. J. Gandía, J. Appl. Phys. **94**, 2417 (2003).
[21] N. F. Mott and E. A. Davis, *Electronic Processes in Non-Crystalline Materials*, 2nd ed. (Oxford University Press, Oxford, 1979).
[22] A. Dussan and R. H. Buitirago, J. Appl. Phys. **97**, 043711 (2005).

Downloaded 18 Apr 2011 to 143.248.224.33. Redistribution subject to AIP license or copyright; see http://apl.aip.org/about/rights_and_permissions